Available online at www.sciencedirect.com
ScienceDirect
Journal of Nuclear Materials 372 (2008) 114–131
journal of nuclear materials
www.elsevier.com/locate/jnucmat

Stress corrosion cracking of low-alloy reactor pressure vessel steels under boiling water reactor conditions

H.P. Seifert *, S. Ritter

Paul Scherrer Institute, Nuclear Energy and Safety Research Department, Laboratory for Materials Behaviour, 5232 Villigen PSI, Switzerland

Received 12 January 2007; accepted 6 March 2007

Abstract

The stress corrosion cracking (SCC) behaviour of different reactor pressure vessel (RPV) steels and weld filler/heat-affected zone materials was characterized under simulated boiling water reactor (BWR) normal water (NWC) and hydrogen water chemistry (HWC) conditions by periodical partial unloading, constant and ripple load tests with pre-cracked fracture mechanics specimens. The experiments were performed in oxygenated or hydrogenated high-purity or sulphate/chloride containing water at temperatures from 150 to 288 °C. In good agreement with field experience, these investigations revealed a very low susceptibility to SCC crack growth and small crack growth rates (<0.6 mm/year) under most BWR/NWC and material conditions. Critical water chemistry, loading and material conditions, which can result in sustained and fast SCC well above the 'BWRVIP-60 SCC disposition lines' were identified, but many of them generally appeared atypical for current optimized BWR power operation practice or modern RPVs. Application of HWC always resulted in a significant reduction of SCC crack growth rates by more than one order of magnitude under these critical system conditions and growth rates dropped well below the 'BWRVIP-60 SCC disposition lines'.
© 2007 Elsevier B.V. All rights reserved.

1. Introduction

The reactor pressure vessel (RPV) of boiling water reactors (BWR) is the most critical pressure-boundary component as far as safety and plant life are concerned [1]. Although most BWR RPV parts are normally protected by a stainless steel cladding with a high resistance against intergranular stress corrosion cracking (SCC), environmentally-assisted cracking (EAC) has to be considered as a potential RPV ageing mechanism, since in safety assessments an incipient crack, which penetrates the cladding has to be assumed. Furthermore, in several BWR cladding was not applied or was removed at some RPV locations, e.g., at the highly stressed feedwater nozzle corner. Additionally, recent SCC cracking incidents related to Inconel 182 weld metal in BWR bottom head penetration housings [2], core shroud support welds [3] and different nozzle safe ends [4] have also drawn the attention to the possibility of SCC in the low-alloy RPV steel. Reliable quantitative SCC crack growth rate data are therefore required for flaw tolerance evaluations and assessments of safety margins and for the verification/adaptation of the intervals of the periodic in-service inspection.

The accumulated operating experience and performance of low-alloy primary pressure-boundary components is very good worldwide [5–10]. Instances of EAC have occurred particularly in BWR service, most often in low-alloy steel (LAS) piping and, very rarely, in the RPV itself [5,8–10]. Oxidizing agents, usually dissolved oxygen (DO), and relevant dynamic straining (e.g., arising from thermal stratification/stripping, thermal and pressurisation cycles during start-up/shut-down, etc.) were always involved [5,8–10]. These cases were attributed either to strain-induced corrosion cracking (SICC) or low-frequency corrosion fatigue (CF) [5,8–10]. Cases with a major contribution of SCC in properly manufactured and heat-treated LAS primary pressure-boundary components are not known to the authors.

* Corresponding author. Tel.: +41 56 310 44 02; fax: +41 56 310 21 99.
E-mail address: hans-peter.seifert@psi.ch (H.P. Seifert).

0022-3115/$ - see front matter © 2007 Elsevier B.V. All rights reserved.
doi:10.1016/j.jnucmat.2007.03.048

Notwithstanding the absence of SCC in RPVs in the field, it has been observed in laboratory tests under simulated BWR conditions with crack growth rates (CGR) ranging from 30 μm/year to 3 m/year under nominally similar testing conditions [11–15]. The SCC behaviour of LAS in oxygenated, high-temperature water and its relevance to BWR power operation, in particular its possible effect on both RPV structural integrity and safety, has therefore been a subject of controversial discussions for many years. Although the overwhelming part of the high SCC CGRs data under pure static loading conditions could be either related to tests with severe violation of small scale yielding conditions, aggressive environmental conditions (e.g., tests in static autoclaves with inadequate water chemistry control and therefore increased levels of chloride and sulphate) or extreme material conditions (e.g., excessive hardness), which cannot be transferred to thick-walled and properly manufactured primary LAS primary pressure-boundary components or appear atypical for current stationary BWR power operation practice, there remained a significant safety concern and uncertainty because of the significant lack of qualified, hard data under plant relevant conditions [7,10].

The SCC crack growth behaviour of different RPV steels and weld metals/weld heat-affected zone (HAZ) materials was therefore investigated under simulated BWR normal water (NWC) and hydrogen water chemistry (HWC) conditions at Paul Scherrer Institute (PSI) within several projects over a very wide range of corrosion system parameters. The present paper is a summary review of the most important phenomenological results and practical aspects of these investigations. A mechanistic interpretation and more detailed information on individual test results can be found in a recent review report [10] and the referenced PSI publications in the individual Sections.

After a brief introduction of the 'BWRVIP-60 SCC disposition lines' [13] (Section 3), the most important effects of mechanical loading, material and environmental parameters on SCC crack growth under simulated BWR/NWC conditions are summarized (Section 4). The adequacy and conservative character of the current 'BWRVIP-60 SCC disposition lines' under BWR conditions are then evaluated and discussed in the context of the PSI results (Section 5). Finally, the mitigation effect of HWC on SCC crack growth is discussed for those critical parameter combinations, where fast stationary SCC was observed under NWC conditions (Section 6).

2. Materials and experimental procedure

2.1. Materials and specimens

Several different types of low-alloy, nuclear grade RPV steels (base metal and HAZ) and a RPV weld filler material were investigated (Tables 1–3). The investigated materials are characteristic for RPVs of Western light water reactors. Concerning the EAC behaviour, the steels mainly differed in their susceptibility to dynamic strain ageing (DSA) and sulphur content/MnS morphology.

All base materials were quenched and tempered. The weld filler, weld HAZ, and some base materials were post-weld heat-treated or stress relieved. The RPV steels had a granular, bainitic (alloy A, C, D, F) or a mixed bainitic/ferritic-pearlitic structure (alloy B) with an average former austenitic grain size of 10–20 μm. The spatial distribution and morphology of the MnS inclusions was fairly homogeneous and similar in alloys A–D covering the range from small, spherical to large (up to a few 100 μm), elongated inclusions. Alloy F revealed distinct banded sulphur segregation zones with large clusters of MnS inclusions. The weld filler material *E* had a very fine-grained, ferritic microstructure with a mean grain size of $\leqslant$6 μm. This material revealed a very fine-dispersed distribution of extremely small ($\leqslant$1 μm), spherical MnS-inclusions. The maximum micro-hardness and tensile residual stress in the region of the HAZ G/H was limited to 350 HV0.5/340 HV0.5 and to 30–40 MPa. The high hardness region with a micro hardness >300 HV0.5 had a significantly larger extension in the weld HAZ H (ca. 2 mm) than in the optimized weld HAZ G (0.5 mm), which is also one reason for the different yield strength levels of the two materials of 880 and 640 MPa.

Twenty-five millimeter thick compact tension specimens (1T C(T)) according to ASTM E399 were used for all experiments. The base metal specimens were manufactured from forged ingots or hot-rolled steel plates mainly in T–L or L–T orientation. The weld metal and weld HAZ specimens were manufactured in the T–L or L–T and T–S or T–L orientation. The specimens were pre-cracked by fatigue in air at room temperature, using a load ratio *R* of 0.1. The maximal K_I at the final load step was $\leqslant$15 MPa $m^{1/2}$. The fatigue pre-crack of the HAZ specimens was positioned in the middle of the HAZ close to the peak hardness region.

2.2. Experimental procedure

The SCC tests were performed in 10 l stainless steel autoclaves with integrated electromechanical loading systems, which were attached to sophisticated refreshing high-temperature water loops (Fig. 1). During the experiments all important mechanical loading (load, pull rod stroke) and environmental parameters at inlet and outlet (DO, DH, κ, *T*, *p*, flow, ...) were recorded continuously. The electrochemical corrosion potential (ECP) of the specimens and the redox potential (platinum probe) were continuously monitored by use of an external Ag/AgCl/0.01 M KCl- or a $Cu/Cu_2O/ZrO_2$-membrane reference electrode. Ionic impurities of the water (inlet and outlet) were analyzed by inductive coupled plasma-atomic emission spectroscopy (ICP-AES) and ion chromatography (IC) about four times each test. Usually, two air fatigue pre-cracked, 25 mm thick compact tension specimens (1T C(T)) were simultaneously tested in a 'daisy chain'. The

Table 1
Overview on investigated low-alloy RPV steels

Material		S (wt%)	Al (wt%)	N_{free} (ppm)	Heat treatment	Microstructure	$R_P^{288°C}$(MPa)	DSA-index
20 MnMoNi 5 5 (≡SA 508 Cl.3)	A	0.004	0.013	30	910–920 °C/6 h/WQ, 640–650 °C/9.5 h/FC	Bainitic	418	−12.3% +++
SA 508 Cl.2 (≡22 NiMoCr 3 7)	B	0.004	0.015	2	900 °C/ 8 h/WQ 600 °C/9 h/AC	Bainitic/ferritic–pearlitic	396	−16.4% +++
SA 533 B Cl.1 (≡20 MnMoNi 5 5)	C	0.018	0.030	<1	915°C/12 h/AC/860 °C/12 h/WQ 660 °C/12 h/FQ/610 °C/40 h/FQ 550 °C/12 h/FQ/550 °C/12 h/FQ	Bainitic	412	−8.9% ++
22 NiMoCr 3 7 (≡SA 508 Cl.2)	D	0.007	0.018	3	890–900 °C/7 h/WQ 640–650 °C/17 h/AC+SR (see material E)	Bainitic	400	−0.58% +
S3 NiMo 1 RPV weld filler	E	0.007	0.005	16	SR: 540–555 °C/59 h/465 °C/ 590–610 °C/21 h/465 °C/ 590–605 °C/11.25 h/AC	Ferritic	430	−2.6% +
20 MnMoNi 5 5 (≡SA 508 Cl. 3)	F	0.015 (0.003–0.053)	0.029	n.m.	900 °C/9 h/WQ/650 °C/34 h/AC/ 660 °C/14 h/AC/550 °C/47 h/600 °C/8 h/AC	Bainitic	439	−9.1% ++
Weld HAZ of D	G	0.007	0.018	n.m.	540–555 °C/59 h/465 °C/ 590–610 °C/21 h/465 °C/ 590–605 °C/11.25 h/AC	–	640	n.m.
Weld HAZ of F	H	0.022	0.015	n.m.	900 °C/9 h/WQ 650 °C/34 h/Air/660 °C/14 h/AC 550 °C/46.5 h/600 °C/8 h/AC	–	850	n.m.

WQ = water quenched, FC = furnace cooled, AC = air cooled, SR = stress relief heat-treatment, n.m. = not measured, DSA-index ($T = 250$ °C) = $(Z_{1E-3\%/s} - Z_{1E-1\%/s})/Z_{1E-1\%/s}$ = ductility loss, +++: high, ++: medium, +: low DSA susceptibility.

Table 2
Chemical composition in wt% of investigated RPV steels and weld filler materials

Material		C	Si	Mn	P	S	Cr	Mo	Ni	V	Al	Cu
20 MnMoNi 5 5	A	0.21	0.25	1.26	0.004	0.004	0.15	0.5	0.77	0.008	0.013	0.06
SA 508 Cl. 2	B	0.21	0.27	0.69	0.005	0.004	0.38	0.63	0.78	0.006	0.015	0.16
SA 533 B Cl. 1	C	0.25	0.24	1.42	0.006	0.018	0.12	0.54	0.62	0.007	0.03	0.15
22 NiMoCr 3 7	D	0.215	0.20	0.91	0.008	0.007	0.42	0.53	0.88	0.007	0.018	0.04
S3 NiMo 1 Weld Filler	E	0.054	0.17	1.19	0.013	0.007	0.04	0.55	0.94	0.006	0.0053	0.06
20 MnMoNi 5 5	F	0.26	0.32	1.44	0.016	0.015	0.15	0.61	0.63	0.02	0.029	0.17
Weld HAZ of D	G	0.215	0.20	0.91	0.008	0.007	0.42	0.53	0.88	0.007	0.018	0.04
Weld HAZ of F	H	0.26	0.32	1.44	0.016	0.022	0.15	0.61	0.63	0.02	0.029	0.17

Table 3
Mechanical tensile test properties of investigated RPV steels and weld materials

Material		25 °C				288 °C
		$R_{P_{0.2}}$ (MPa)	R_m (MPa)	A_5 (%)	Z (%)	$R_{P_{0.2}}$ (MPa)
20 MnMoNi 5 5	A	485	648	19.3	72.1	418
SA 508 Cl. 2	B	448	611	17.9	71.0	396
SA 533 B Cl. 1	C	456	605	23.4	59.9	412
22 NiMoCr 3 7	D	467	600	17.3	71.9	400
S3 NiMo 1 Weld Filler	E	492	592	17.4	73.3	430
20 MnMoNi 5 5	F	508	664	20	61	439
Weld HAZ of D	G	640*	–	–	–	–
Weld HAZ of F	H	880	910	–	–	–

$R_{P0.2}$: yield strength, R_m: ultimate tensile strength, A_5: uniform elongation, Z: reduction of area, * = with instrumented hardness tester.

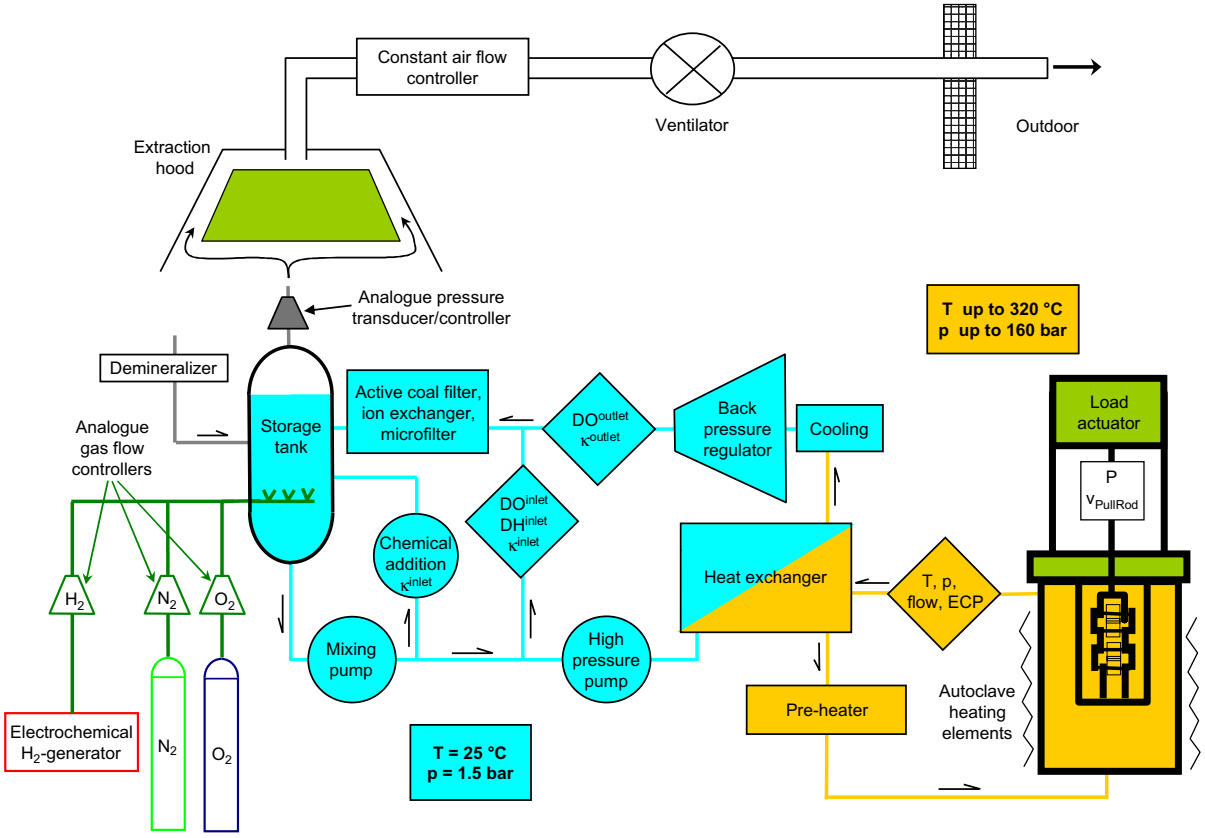

Fig. 1. Schematic of high-temperature water loop with autoclave and electro-mechanical tensile machine.

crack advance was continuously monitored using the reversed direct current potential drop (DCPD) method with a resolution limit of about 2 μm. After the tests all specimens were broken open at liquid nitrogen temperature

for fractographical analysis in the scanning electron microscope (SEM).

The different phases of the SCC experiments and loading conditions are shown in Fig. 2 and Table 4. The specimens were first pre-oxidized in the test environment at a small constant pre-load for one week. Then in all tests either a cyclic loading phase with a positive saw tooth waveform (slow loading, fast unloading) with a constant load amplitude or a slow rising load phase with constant load rate was applied to obtain an actively growing EAC crack before switching to periodical partial unloading, constant or ripple loading.

BWR conditions were mostly simulated with high-purity (inlet/outlet conductivity κ of $<0.06/<0.1$ μS/cm, ionic impurities <1 ppb), hydrogenated (HWC) or oxygenated (NWC) water at a temperature of 288 °C. In some few cases mixtures of hydrogen and oxygen with stoichiometric oxygen or hydrogen excess were used. For HWC conditions, a dissolved hydrogen (DH) content of 150 ppb was usually applied resulting in a redox-potential and an ECP of -530 and -550 to $-600\,mV_{SHE}$, respectively. For NWC conditions, the ECP (and dissolved oxygen (DO) content) was varied between -100 (50 ppb DO) and $+200\,mV_{SHE}$ (8000 ppb DO). In most tests a DO content of 400 or 8000 ppb was applied. A DO of 400 ppb (ECP $= +50\,mV_{SHE}$, redox-potential $= +250\,mV_{SHE}$) represents the total oxidant concentration in the reactor water during BWR steady-state power operation in a realistic way. The increased DO value of 8000 ppb (ECP $= +150\,mV_{SHE}$, redox-potential $= +290\,mV_{SHE}$) was applied to achieve a realistic ECP of $+150\,mV_{SHE}$ for a surface crack penetrating the stainless steel cladding on the RPV wall/nozzles. These conditions may appear to be overly aggressive/conservative for many other LAS BWR pressure-boundary components (e.g., feedwater piping or piping with flowing steam). To simulate conditions in other LAS pressure-boundary components (e.g., feedwater piping or RPV feedwater nozzle) or water chemistry transients during BWR power operating conditions, additional tests at temperatures of 150, 200, 250 or 288 °C were performed as well as sulphate or chloride in terms of Na_2SO_4/H_2SO_4 or NaCl/HCl, respectively, were added to the high-purity water in some experiments. All tests were performed under low-flow conditions (4–5 autoclave

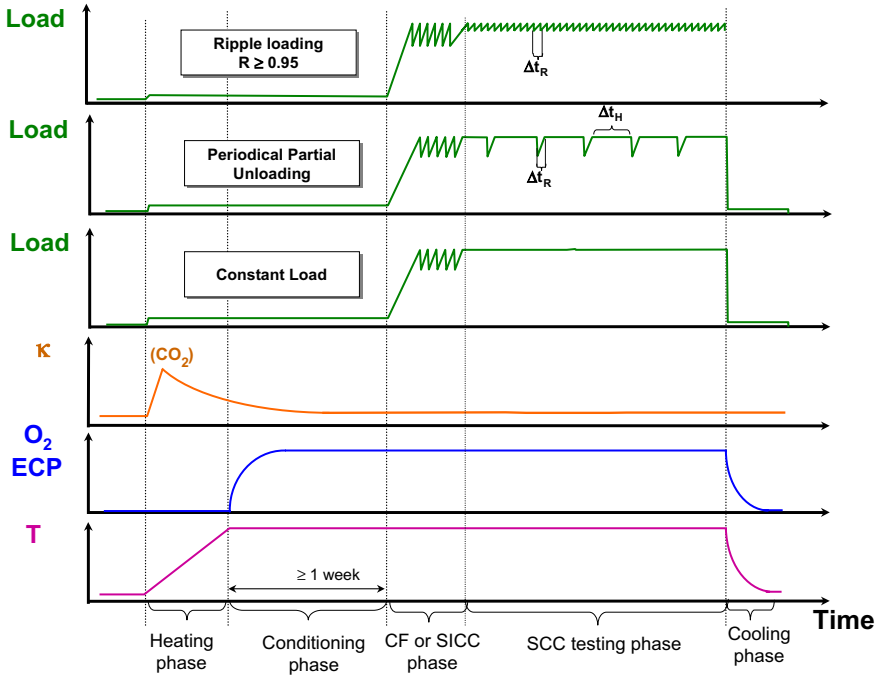

Fig. 2. Simplified schematic of applied test procedures for SCC experiments in high-purity high-temperature water.

Table 4
Summary of loading conditions for SCC experiments

	Constant load	Periodical partial unloading	Ripple loading
$R = P_{min}/P_{max}$ (–)	1	0.8, 0.7 or 0.2	0.95 to 0.98
K_I or K_I^{max} (MPa m$^{1/2}$)	15–105	30 to 70	30 to 80
Δt_{Rise} (s)	–	100, 500, 1000 or 4000	12–10^5
Δt_{Hold} (s)	$\Delta t_{Constant\ load} = 200$–2000 h, usually 1000 h	0–10^5	–
Preceding loading step(s)	Low-frequency fatigue or slow rising load or periodical partial unloading	Low-frequency fatigue	Low-frequency fatigue with stepwise increase of R

exchanges per hour) with a local flow rate of some few mm/s to generate conservative data with respect to most plant locations with turbulent high-flow conditions.

3. BWRVIP-60 SCC disposition lines

Based on the results of recent SCC tests under simulated BWR conditions [11–13,15] and the critical review of older literature data and the field experience, disposition lines for SCC crack growth in LAS during BWR power operation were proposed by an international group of experts, working within the framework of the 'BWRVIP project' of the Electric Power Research Institute (EPRI), and accepted by the US Nuclear Regulatory Commission (NRC) as an interim position (Fig. 3) [13]. The 'BWRVIP 60 SCC disposition line 1' applies to crack growth in LAS under static loading and transient-free, stationary BWR/NWC or HWC power operation conditions. The 'BWRVIP-60 disposition line 2' (='low-sulphur SCC line' of the General Electric model [7,14]), on the other hand, may be used for estimating SCC crack growth during and 100 h after transients in water chemistry ('EPRI action level 1 limit' of EPRI BWR water chemistry guidelines [16,17]) or load transients not covered by fatigue evaluation procedures.

4. SCC crack growth behaviour under BWR/NWC conditions

4.1. Effect of loading conditions

4.1.1. Constant loading – effect of stress intensity factor K_I

The effect of K_I on SCC crack growth under constant load was investigated in chloride-free, oxygenated high-temperature water (DO = 200–8000 ppb, ECP = −50 to +150 mV_{SHE}) at 274 and 288 °C and is summarized in Figs. 4–7 and Table 5. Under these conditions, all investigated materials with the exception of the HAZ H (see Section 4.2.3) showed no or only minor SCC crack growth even in tests with aggressive environmental parameters (65 ppb SO_4^{2-}, ECP = +150 mV_{SHE}) at stress intensities $K_I < 60$ MPa $m^{1/2}$. The crack growth of fast growing transgranular

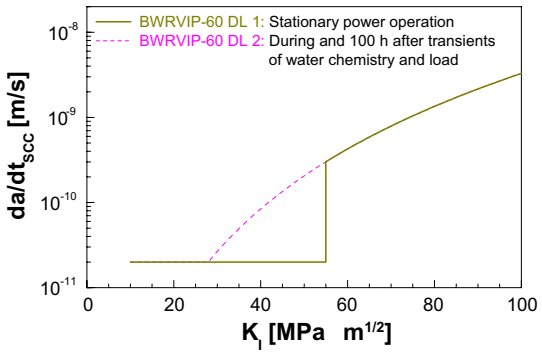

Fig. 3. 'BWRVIP-60 SCC disposition lines' [13].

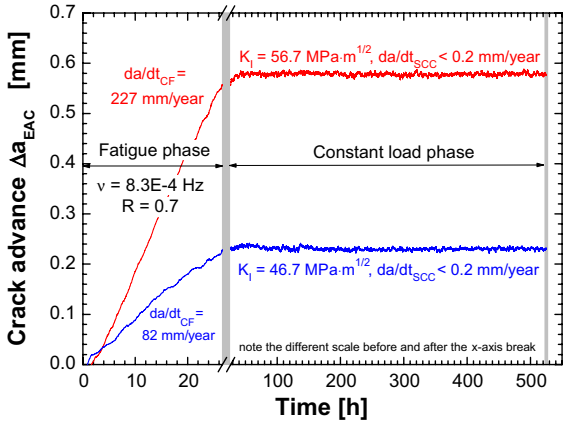

Fig. 4. Example of combined low-frequency corrosion fatigue → constant load test in oxygenated, high-purity high-temperature water, which confirms cessation of SCC briefly after switching to constant load [10].

EAC cracks (3E−10 to 3E−7 m/s), triggered by slow rising load or low-frequency fatigue loading (Fig. 4) at the beginning of the tests either slowed down to CGRs of less than 0.6 mm/year or arrested within a few hundred hours under constant load in case of stress intensities $K_I < 60$ MPa $m^{1/2}$ [10,11,15].

Below 30 MPa $m^{1/2}$ almost instantaneous crack arrest occurred after switching to constant load. Between 30 and 60 MPa $m^{1/2}$ the SCC crack growth either slowed down to CGRs of less than 0.6 mm/year or arrested within a few hundred hours under constant load. The SCC crack growth under these conditions (if it occurred at all) was usually very localized (some few isolated locations with very limited crack growth, often around MnS-inclusions which were intersected by the crack front, Fig. 8) and could usually only be detected by post-test fractography with some very few exceptions. Because of the extremely low susceptibility to SCC crack growth under these conditions, no effect of K_I on SCC CGRs could be resolved below 60 MPa $m^{1/2}$.

Sustained transgranular SCC crack growth was only observed above 60 MPa $m^{1/2}$ and the SCC CGRs tended to increase with increasing K_I values (Fig. 5), although in many cases they were still decaying with time following roughly a reciprocal time law (logarithmic law for crack growth, Fig. 6). Stationary SCC crack growth was only observed at extremely high loading conditions ($K_I \geqslant 80$ MPa $m^{1/2}$) if the K_I or the load approached either the K_{IJ} value of the material or the plastic limit load (Fig. 5). To date, it is not fully clear, to which extent the transition from very slow to sustained accelerated SCC crack growth is relevantly affected (and shifted to lower K_I-values) by the loss of constraint in this high K_I-regime in small specimens with severe violation of small scale yielding conditions.

In summary, all materials (with the exception of HAZ H) revealed a very similar SCC crack growth behaviour in chloride-free high-temperature water at 274–288 °C with CGRs well below the 'BWRVIP-60 SCC disposition line 1' (Fig. 7) as long as K_I were limited to values <60 MPa $m^{1/2}$

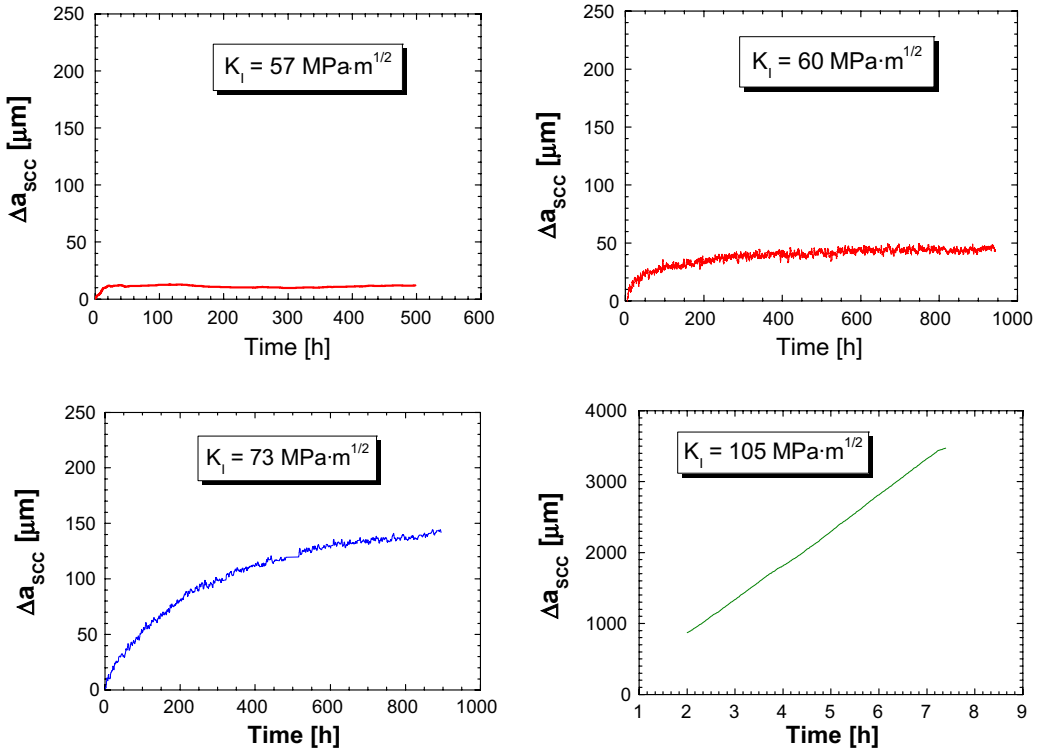

Fig. 5. Examples of SCC crack growth in high-sulphur RPV steel C (0.018 wt% S) at 288 °C and different K_I levels under aggressive environmental conditions (8 ppm DO, 65 ppb SO_4^{2-}) after switching from low-frequency fatigue to constant load [10].

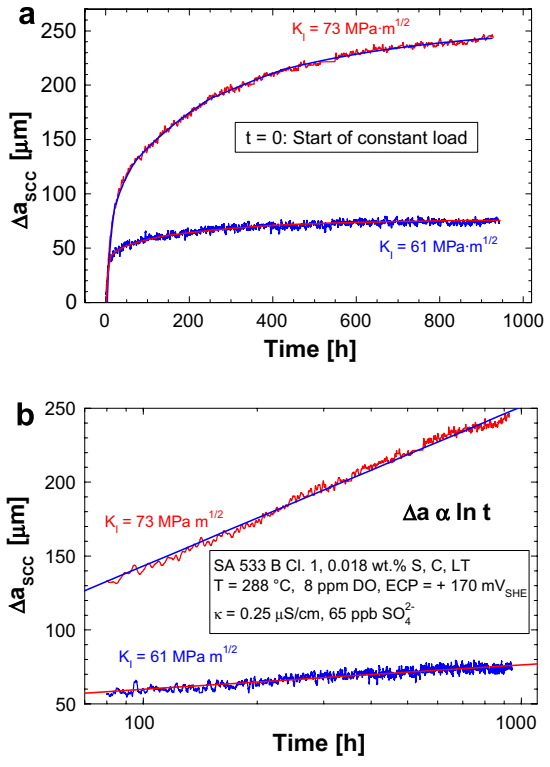

Fig. 6. Decay of SCC crack growth according to logarithmic time law, which indicates that SCC and crack-tip strain rate are controlled by low-temperature creep under these specific conditions [10,11].

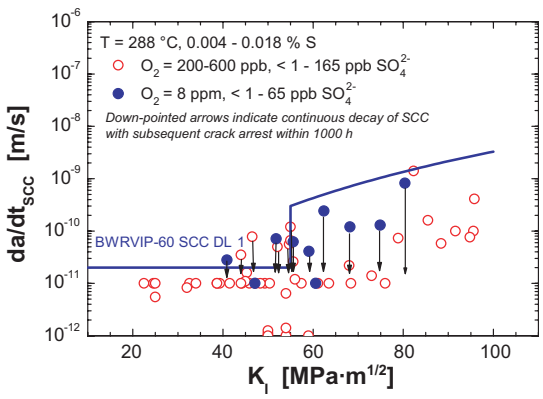

Fig. 7. Confirmation of the conservative character of the BWRVIP-60 SCC DL 1 for stationary, transient-free BWR power operation by combined slow rising load/low-frequency fatigue → constant load tests in chloride-free, oxygenated high-temperature water at 274 to 288 °C [10,11,15].

[10,11,15]. Even above 60 MPa $m^{1/2}$, most test SCC CGR results, in particular with low- and medium-sulphur RPV steels, were still below 'BWRVIP-60 SCC disposition line 1'. The PSI data thus support the adequacy and conservative character of this interim disposition line for the RPV during stationary BWR/NWC power operation. The conservative character at 288 °C was further confirmed by

Table 5
Summary of PSI constant load SCC crack growth results in chloride-free oxygenated, high-temperature water at 274–288 °C with 1T C(T) specimens [10,11,15]

K_I (MPa $m^{1/2}$)	Region	SCC crack growth under constant load	Mean SCC crack growth rate during the constant load period of 1000 h (m/s)	SCC crack growth rate after 1000 h (m/s)
<30	SSY	No crack growth	$<6\times10^{-12}$*	$<6\times10^{-12}$*
30–60	≈SSY	Strictly limited in time ≈10^1 h – ≈10^2 h	$<2\times10^{-11}$	$<6\times10^{-12}$*
60–80	Transition region	Limited in time ≈10^2 h – ≈10^3 h	$<3\times10^{-10}$	$<3\times10^{-11}$
⩾80 $K_I \rightarrow K_{IJ}$**	Ligament yielding	Yes, sustained, stationary in some cases	$>3\times10^{-10}$ $<3\times10^{-7}$	$>3\times10^{-10}$ $<3\times10^{-7}$

Sulphur (wt%)	SICC or CF crack growth rate prior to constant load phase (m/s)	T (°C)	κ (μS/cm)	Cl^- (ppb)	SO_4^{2-} (ppb)	ECP (mV_{SHE})	DO (ppm)
0.004–0.018	3×10^{-10} to 3×10^{-7}	274–288	0.06–1.0	<1–2	<1–365	0–200	0.2–8

SSY: small scale yielding.
* ⩽Detection limit.
** $K_{IJ} = (J_i \cdot E/(1-\nu^2))^{1/2}$.

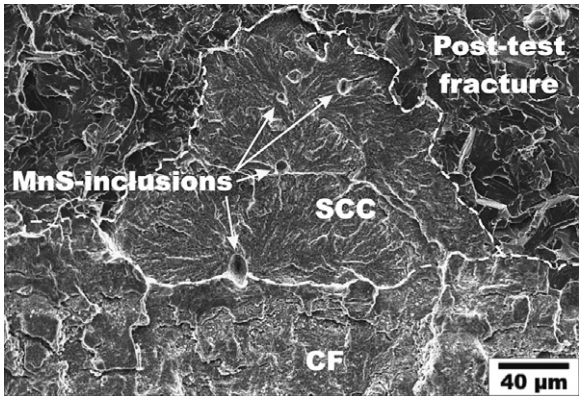

Fig. 8. Localized SCC crack growth under constant load due to MnS-inclusions, intersected by the crack front.

European Round Robin tests [18–20] and long-term reactor site testing [13,21].

4.1.2. Periodical partial unloading

In order to further confirm the observed SCC cracking behaviour and the conservative character of the 'BWRVIP-60 disposition line 1', the effect of periodical partial unloading on SCC crack growth was investigated in oxygenated, high-purity high-temperature water with a DO of 400 or 8000 ppb at a temperature of 288 or 250/240 °C. Additional tests were performed with high-temperature water containing 65–365 ppb sulphate and 5–50 ppb chloride. The loading conditions are summarized in Table 4 [10,19].

For $K_{I,max}$ values <60 MPa $m^{1/2}$ and chloride contents <5 ppb, the time-based CGRs da/dt_{SCC} always decreased with increasing hold time Δt_H for all material and loading conditions (Fig. 9(a)). Above a hold time of 1–20 h (depending on $K_{I,max}$-values, rise times Δt_R, temperatures, ECP, ...) the CGRs generally dropped below the current 'BWRVIP-60 SCC disposition line 1 and 2' (Fig. 9(b)), thus further confirming their conservative character. At hold

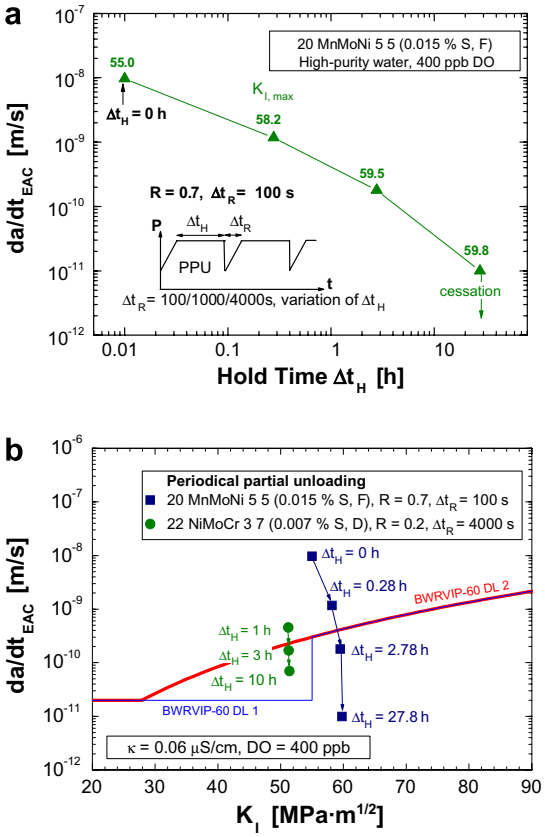

Fig. 9. (a) Example of effect of hold time on time-based EAC CGRs in PPU tests and (b) comparison with the BWRVIP-60 SCC DLs [10].

times ⩾10 h the time-based SCC CGRs generally dropped below the detection limit of the DCPD of 6E−12 m/s.

For $K_{I,max}$ values <60 MPa $m^{1/2}$ and chloride contents <5 ppb, the crack advance per cycle $\Delta a/\Delta N_{EAC}$ did not depend on the hold time for a fixed rise time (Fig. 10(a)) and was identical to that under cyclic saw tooth loading conditions with the same rise time. This behaviour could be related to the absence of any relevant SCC crack growth

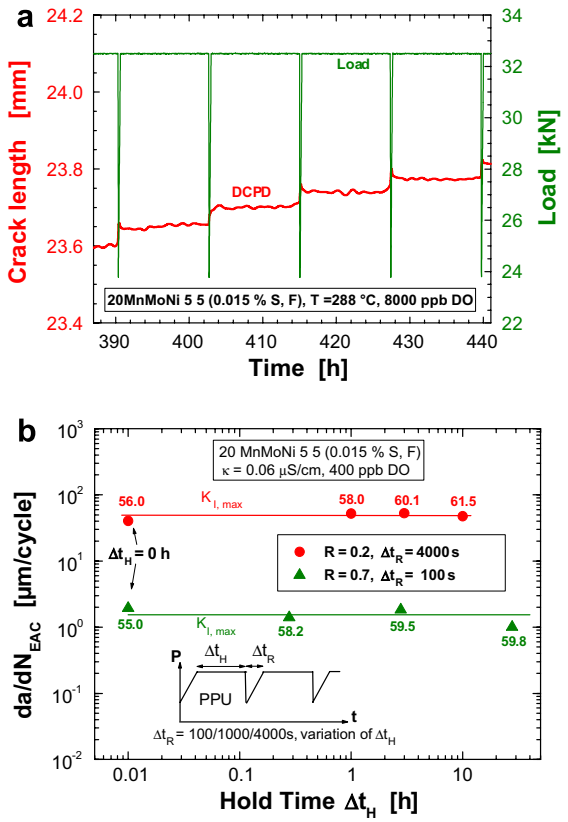

Fig. 10. EAC crack growth during PPU and effect of hold time Δt_H on the crack advance per PPU cycle. Both plots clearly show that the crack is only growing during the rising load phase by SICC without any significant SCC contribution during the constant load phases of the PPU cycles [10].

at constant load under these conditions. As shown in Fig. 10(b), EAC crack growth only occurred during the rising load phase by SCC with no SCC during the subsequent constant load phase of the trapezoidal fatigue cycle. The PPU tests therefore also basically confirmed the observed EAC cracking behaviour in combined rising load/low-frequency fatigue → constant load tests (see Section 4.1.1).

An increase of $\Delta a/\Delta N_{EAC}$ with hold time Δt_H was only observed under some very specific system conditions, where sustained SCC was usually observed in constant load tests in LAS, e.g., for chloride contents $\geqslant 5$ ppb (see Section 4.3.3), high $K_{I,max}$ values > 60–70 MPa $m^{1/2}$ (Section 4.1.1), high hardness $\geqslant 350$ HV5 (Section 4.2.3) or at intermediate temperatures in materials with a high DSA susceptibility (Section 4.2.2). On the other hand, in some isolated cases, in particular at low $K_{I,max}$ values and low load-ratios, a decrease of $\Delta a/\Delta N_{EAC}$ with increasing hold time Δt_H and cessation of EAC has been observed for long hold times $\geqslant 10$ h, which was probably caused by oxide- or surface roughness-induced crack closure.

4.1.3. Ripple loading

The possible effect of small load fluctuations at very high load ratios ($R \geqslant 0.95$) near to the fatigue threshold ΔK_{th} of 1–2 MPa $m^{1/2}$ ('ripple loading') on SCC crack growth was investigated in high-purity (<1 ppb SO_4^{2-}, $\kappa \leqslant 0.06$ µS/cm), high-temperature water at 288, 274 and 250 °C with a DO of 8000 (+150–200 mV_{SHE}) and 400 ppb (+50 mV_{SHE}). The loading conditions are summarized in Table 4 [10,15].

In Fig. 11 the EAC CGRs of the ripple load tests are compared to the 'BWRVIP-60 SCC disposition line 2', which should conservatively cover the EAC crack growth under such loading conditions. In all investigated materials sustained, stationary EAC crack growth was observed in high-temperature water with a DO of 8000 and 400 ppb in the loading frequency range from 10^{-2} to 10^{-4} Hz. The SCC CGRs thereby reached values up to 30–160 mm/year at stress intensity factors between 30 and 76 MPa $m^{1/2}$. The maximum EAC CGRs under ripple loading conditions were similar for a DO of 400 and 8000 ppb and for the different materials and did not significantly depend on the stress intensity factor in the range from 30 to 76 MPa $m^{1/2}$. Ripple load investigations of Argonne National Laboratory (ANL) revealed a very similar EAC behaviour with CGRs up to 250 mm/year in the stress intensity factor range of 30–70 MPa $m^{1/2}$ [22].

At ΔK values $\geqslant 2$ MPa $m^{1/2}$, the ripple loading in the frequency range of 10^{-2}–10^{-4} Hz resulted in EAC crack growth, which was a factor of up to 150 faster than the corresponding SCC crack growth under pure static loading conditions at identical K_I levels and environmental conditions (Fig. 11). Even for small stress intensity factors of 30 MPa $m^{1/2}$ and DO of 400 ppb, the maximum EAC CGRs significantly exceeded the 'BWRVIP-60 SCC disposition line 2', which thus does not conservatively cover the EAC crack growth behaviour under these loading conditions. If the ΔK value or loading frequency were reduced to values $\leqslant$1.5–2 MPa $m^{1/2}$ and $\leqslant 10^{-5}$ Hz, cessation of EAC crack growth below the 'BWR VIP SCC disposition line 1' and subsequent crack arrest was observed (Fig. 12).

The EAC crack growth behaviour and the observed parameter trends (e.g., effect of ΔK and frequency (Fig. 12)) under ripple load conditions excellently correlated with the corrosion fatigue behaviour of these materials in other PSI investigations [10]. A detailed analysis

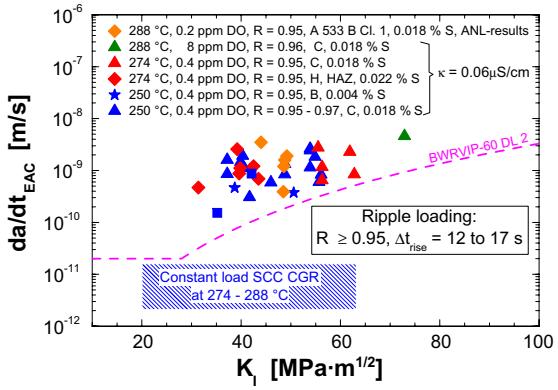

Fig. 11. Comparison of time-based EAC CGRs in oxygenated, high-purity, high-temperature water in different RPV steels under ripple loading conditions ($R \geqslant 0.95$) with BWRVIP-60 SCC DL 2 for load and water chemistry transients [10].

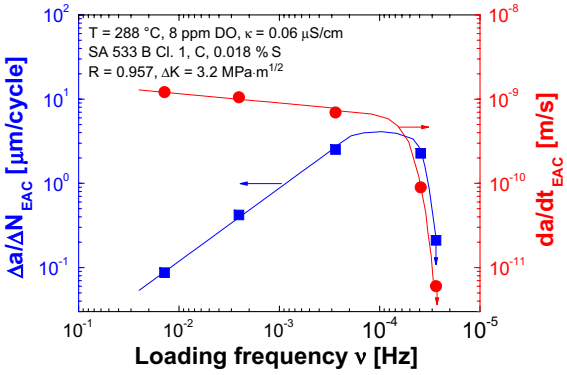

Fig. 12. Effect of loading frequency on time-based and cycle-based EAC CGRs in the high-sulphur RPV steel C in oxygenated, high-purity, high-temperature water under ripple loading conditions at $R = 0.957$. Cessation of EAC is observed below a loading frequency of 10^{-4} Hz [10].

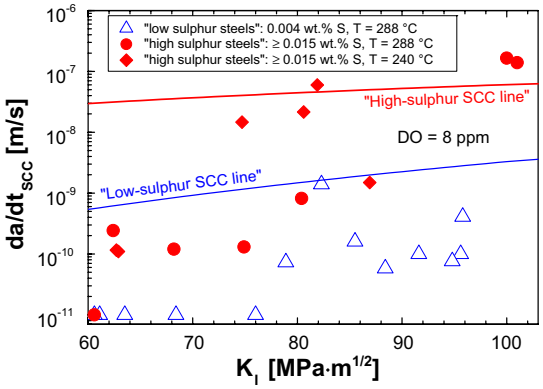

Fig. 13. Tendency for higher SCC CGR with increasing steel sulphur content at K_I-values >60 MPa $m^{1/2}$.

revealed that EAC under these loading conditions may be fully understood as normal corrosion fatigue at small ΔK and high load ratio R without any significant SCC contribution at $K_I < 60$ MPa $m^{1/2}$ [10]. The observed EAC cracking behaviour under ripple loading conditions is thus fully consistent with that in tests with constant load or periodical partial unloading and further confirms the low SCC crack growth susceptibility. It is stressed that also the current cycle-based 'ASME XI wet reference (corrosion) fatigue crack growth curves' do not conservatively and adequately cover the EAC crack growth under these conditions.

Although ripple loading is not relevant for large pressure vessels such as the RPV, similar loading conditions might occur in specific pipe (or nozzle) sections close to pumps or in locations, where thermal stripping can occur, in particular in combination with superimposed weld residual tensile stresses. Here, the observed behaviour should be verified by further ripple load tests at slightly lower ECPs with lower K_I and ΔK levels and, in particular, at higher and more relevant loading frequencies of 0.1–10 Hz.

4.2. Effect of material parameters

4.2.1. Effect of steel sulphur content and MnS-inclusions

Since SCC crack growth could not be sustained in chloride-free, oxygenated high-temperature water at 274–288 °C up to relatively high K_I values of 60 MPa $m^{1/2}$, no effect of steel sulphur content (and of any other material parameter) could be derived in this K_I and temperature range. Nevertheless, above 60 MPa $m^{1/2}$ there were some weak indications that the transition from these low to high SCC CGRs was shifted to lower K_I values with increasing steel sulphur content and that high-sulphur steels tended to produce higher SCC CGRs in this region [10,11] (Fig. 13).

In spite of the absence of any significant effect of steel sulphur content on SCC crack growth in high-purity water at K_I-values below 60 MPa $m^{1/2}$, which may be related to the cessation behaviour under constant load, a low steel sulphur content is still very beneficial: A lower sulphur content usually results in a lower EAC initiation susceptibility in many cases [10]. Furthermore, the higher toughness of these low-sulphur steels always results in higher allowable/critical crack sizes, and hence in higher structural integrity safety margins.

4.2.2. Effect of dynamic strain ageing

In LAS, the dynamic strain ageing (DSA) phenomenon is usually observed during plastic straining at sufficient slow strain rates ($\leqslant 10^{-2}$ s^{-1}) in the temperature range from 100 to 350 °C and is related to an elastic interaction between the strain fields of solute interstitials as nitrogen and carbon and moving dislocations [10,23]. Within the DSA temperature-strain rate range, the localisation of plastic deformation by DSA facilitates the mechanical rupture of the protecting oxide film. Additionally, the increase of the yield strength, strain hardening exponent and low temperature creep rate by DSA results in a higher crack-tip strain and strain rate than for identical loading conditions outside the DSA range, or than in a material which is not (or less) susceptible to DSA.

The investigations on temperature effects (see Section 4.3.2) clearly revealed a relevant effect of DSA on SCC crack growth in LAS at intermediate temperatures (180–270 °C), which even seemed to dominate steel sulphur effects [10,12]. The effect of DSA on SCC is exemplarily illustrated in Figs. 14–16. At intermediate temperatures, a different SCC behaviour was observed in LAS with low and high DSA susceptibilities (Fig. 14). In contrast to 288 °C (see Section 4.1.1), stationary accelerated SCC with CGRs in the range or slightly above the 'BWRVIP-60 disposition line 1' was observed in the low-sulphur alloys A and B with a high DSA susceptibility, which was a factor of 50–600 times faster than in the high-sulphur alloy C with a moderate DSA susceptibility. A good coincidence of the maximum in SCC CGRs at intermediate temperatures, derived from constant load tests under low-flow, oxygenated high-temperature water conditions and the minimum in reduction of area (maximum in DSA-susceptibility),

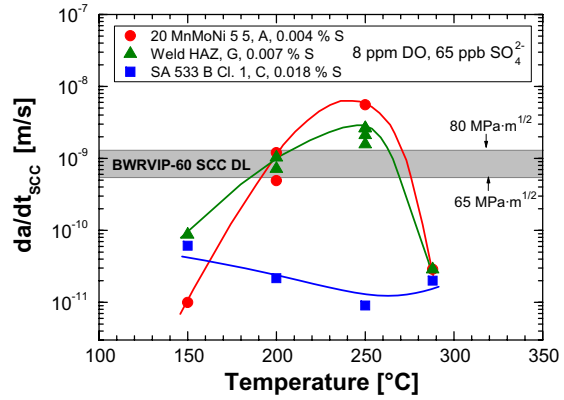

Fig. 14. Effect of temperature on SCC CGRs.

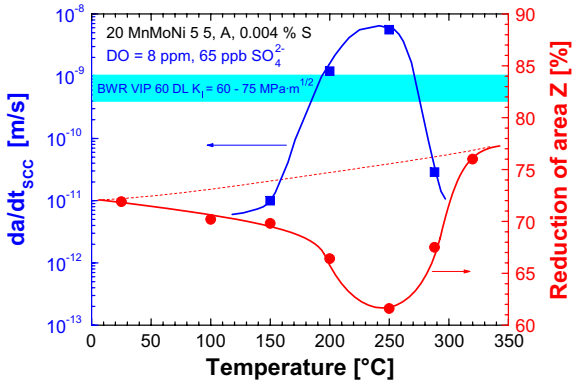

Fig. 15. Coincidence between maximum in SCC CGRs with DSA in terms of temperature for the RPV steel A with high DSA susceptibility [15].

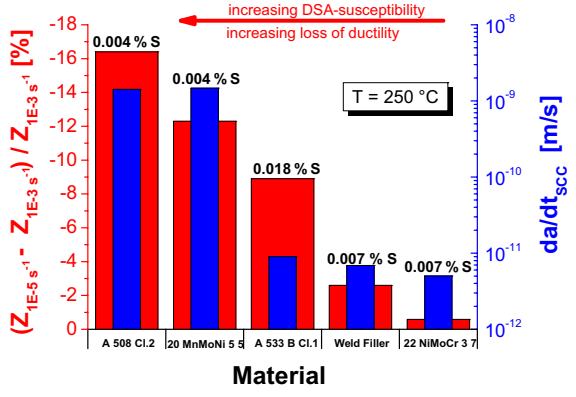

Fig. 16. Good correlation between degree of DSA susceptibility and SCC CGRs at intermediate temperatures in different LAS [15].

measured in tensile tests in air at similar strain rates, was observed in LAS with a high DSA susceptibility (Fig. 15) [10,13]. Furthermore, the SCC CGRs at 250 °C correlated roughly with the DSA-susceptibility of the different materials (Fig. 16), further confirming the possible effect of DSA [10,13].

Although the typical stationary BWR RPV operation temperature of 274–288 °C is slightly above the most critical temperature range of 200–250 °C, the finding of sustained SCC at intermediate temperatures in LAS with a high DSA susceptibility may be of relevance for other BWR LAS pressure-boundary components like the feedwater piping system (200–220 °C), the RPV feedwater nozzles or the condensate piping system with lower operation temperatures. The effect of DSA should therefore be further investigated at slightly lower ECPs than in the present experiments, which are more representative for these components. In contrast to the steel sulphur content, the DSA susceptibility of LAS pressure-boundary components is usually not known. Although chemical composition and manufacturing process can give a first rough indication about the possible degree of DSA susceptibility of the steel, destructive methods like internal friction measurements or tensile tests at different temperatures and strain rates are currently still required for its quantification.

4.2.3. Effect of yield strength and hardness

Different yield strength/hardness levels in the high-sulphur steel C were produced by various heat-treatments (Table 6), which did not affect the MnS-morphology. Besides the bainitic microstructure ($Q + T$), which is characteristic for the RPV base metal, a martensitic (Q) and a ferritic–pearlitic microstructure (N) were produced by austenizing/water quenching and austenizing/slow furnace cooling. The SCC crack growth behaviour of these microstructures in oxygenated, high-temperature water with a DO of 8000 ppb was then further compared to the weld metal E and the weld HAZ materials G and H with different yield strength/hardness, but also different sulphur contents and DSA susceptibilities (whereas DSA effects are expected to be moderate at 288 °C) [10,15].

At 288 °C, the same SCC behaviour with cessation of crack growth and CGRs <0.6 mm/a at $K_I \leqslant 70$ MPa $m^{1/2}$ was observed for the ferritic–pearlitic and bainitic microstructure as described in Section 4.1.1. On the other hand, the specimen with the martensitic microstructure (with an excessive hardness of 466 HV5) revealed stationary, fast SCC crack growth with a CGRs of up to 6000 mm/year in the K_I-range from 64 to 84 MPa $m^{1/2}$.

Fig. 17(a) and (b) show the effect of hardness and yield strength on the SCC CGRs at 288 °C in high-temperature water with 8000 ppb DO in the K_I-range from 50 to 65 MPa $m^{1/2}$. Micro hardness values of the peak hardness region were used for the two weld HAZ materials, since the crack planes were located in this region. In this K_I-range, the different LAS (see Tables 1–3) and microstructures revealed a similar SCC crack growth behaviour with SCC CGRs below the 'BWRVIP-60 SCC disposition line 1' up to a critical hardness and yield strength level of roughly 350 HV5 and 800 MPa. Above this threshold, stationary, accelerated SCC above the 'BWRVIP-60 disposition line 1' was observed and for extremely high hardness values >450 HV5 the SCC CGRs even exceeded the 'high-sulphur SCC line' of the General Electric model [7,14]. In contrast to the optimized weld HAZ G, the weld HAZ H with a

Table 6
Applied heat treatments and resulting properties of the RPV steel C

Parameter	$Q+T$	N	Q
Heat treatment	915 °C/12 h/Air/860 °C/12 h/WQ 660 °C/12 h/FQ/610 °C/40 h/FQ 550 °C/12 h/FQ/550 °C/12 h/FQ	900 °C/30 min/FQ	900 °C/30 min/WQ
Microstructure	Bainitic	Ferritic–pearlitic	Martensitic
Vickers hardness	197 HV10	260 HV10	466 HV10
$R_P^{288\ °C}$	411 MPa	577 MPa	960 MPa

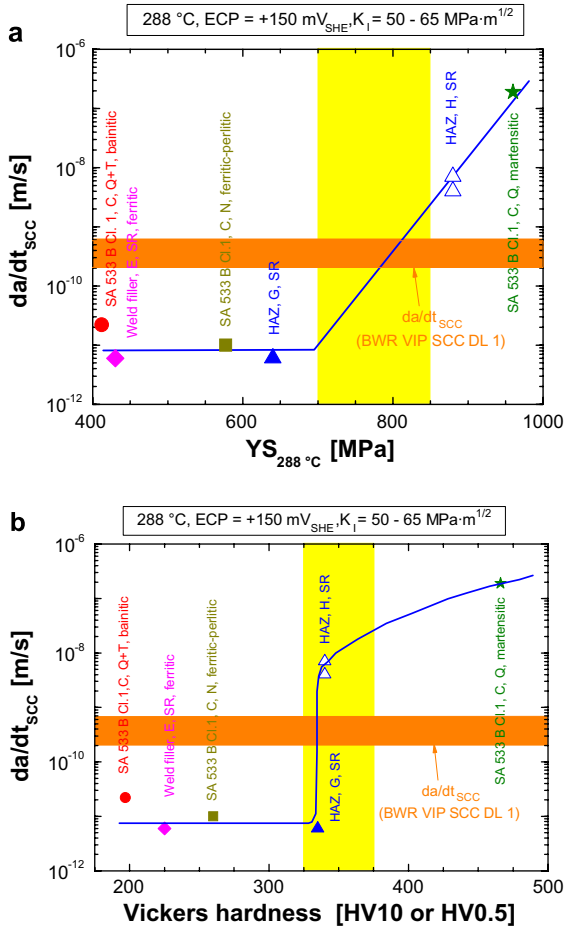

Fig. 17. Effect of yield strength (a) and hardness (b) on SCC CGRs in different LAS.

significantly higher yield strength of 880 MPa and sulphur content of 0.022 wt% S (but comparable peak micro hardness) revealed fast SCC above the 'BWRVIP-60 disposition line 1' down to stress intensity factors of 35 MPa m$^{1/2}$ even in high-purity water with a DO of 400 ppb (Fig. 22) in spite of similar peak micro hardness.

Critical hardness and yield strength levels for SCC are usually not achieved in properly manufactured LAS primary pressure-boundary components. The hardness of weld HAZ is controlled and limited to values <350 HV5 by quality assurance measures/careful selection of welding parameters/post weld heat treatment and cold work (bending) and the degree of cold work, which can be accepted without any heat treatment is also strictly limited. But critical conditions and a high SCC susceptibility might occur in case of weld fabrication deficiencies or of repair welding without post-weld heat treatment.

4.3. Effect of environmental parameters

4.3.1. Effect of corrosion potential and dissolved oxygen content

The effect of DO/ECP in the range from 50 to 8000 ppb and −100 to +150 mV$_{SHE}$ was investigated in high-purity or sulphate-containing (up to 370 ppb SO_4^{2-}) high-temperature water at 288 or 274 °C [10,11,15].

As long as K_I and the Vickers hardness/sulphur content were limited to values <60 MPa m$^{1/2}$ and <350 HV5/<0.02 wt%, all materials revealed a very similar SCC crack growth behaviour in this ECP/DO range at 274 or 288 °C with CGRs well below the 'BWRVIP-60 disposition line 1' (Figs. 7 and 18). The observed behaviour was additionally confirmed in high-purity or sulphate-containing high-temperature water with a DO and DH of 400 ppb and 25 ppb (stoichiometric excess of oxygen) at an ECP of +30–50 mV$_{SHE}$ (Fig. 18). The similar behaviour over the whole ECP range may be related to the SCC cessation behaviour and the extremely low SCC crack growth susceptibility under these conditions. The potentially strong effect of ECP/DO on SCC is therefore better seen in Fig. 21 in Section 4.3.3, where the critical chloride concentration for the onset of accelerated SCC is decreasing with increasing ECP. Above 60 MPa m$^{1/2}$ there were not enough

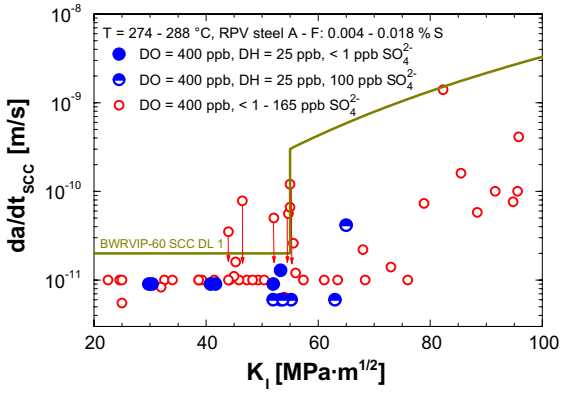

Fig. 18. Similar SCC CGRs in high-temperature water with oxygen and oxygen/hydrogen mixtures with stoichiometric oxygen excess.

data to reveal a clear data trend, although it is expected the transition to high SCC CGRs is shifted to lower K_I-values with increasing ECP/DO content [10].

4.3.2. Effect of temperature

The effect of temperature on the SCC crack growth was investigated with selected materials between 150 and 288 °C. The tests were conducted in oxygenated high-temperature water with 8000 ppb DO and either 65 ppb or <1 ppb SO_4^{2-}. The ECP decreased from +250 mV_{SHE} at 150 °C to +150 mV_{SHE} at 288 °C. Additional controlling tests in high-purity with a DO of 400 ppb were performed at 200–288 °C [10,15].

The effect of temperature was dependent on the material and is illustrated in Figs. 14 and 15. At a temperature of 274–288 °C, all investigated materials (<350 HV5/ < 0.02 wt% S) showed no or only minor SCC crack growth (<0.6 mm/a) at $K_I < 60$ MPa $m^{1/2}$ (see Sections 4.1 and 4.2).

The SCC crack growth behaviour of the high-sulphur RPV steel C with moderate DSA susceptibility revealed the same SCC crack growth behaviour and similar CGRs over the whole temperature range (150–250 °C) as at 288 °C (Fig. 15) and the SCC CGRs were below the 'BWR VIP 60 SCC disposition line 1' at all temperatures even for K_I values of up to 80 MPa $m^{1/2}$.

At intermediate temperatures of 200 and 250 °C the low-sulphur RPV steels A and B with the high DSA susceptibility and the weld HAZ material H and G revealed a totally different SCC behaviour. Sustained, stationary SCC with CGRs in the range or slightly above the 'BWRVIP-60 SCC disposition line 1' were observed (Fig. 22, Section 5). At 150 °C, these materials revealed again the same behaviour as at 288 °C. As discussed in Section 4.2.2, the maximum SCC CGRs at intermediate temperatures of 200 to 250 °C may be related to DSA and to the different DSA susceptibilities of the steels, respectively.

The materials thus either showed a low SCC crack growth susceptibility over the whole investigated temperature range from 150 to 288 °C (RPV steel C) or a maximum of SCC CGRs at intermediate temperatures between 180 and 270 °C (RPV steel A/B and weld HAZ G/H).

4.3.3. Effect of sulphate and chloride

Although BWRs are usually operated with neutral high-purity water and the concentration of harmful anionic species like sulphate and chloride is usually below 1 ppb during stationary power operation, increased transient levels of sulphate and chloride >5 ppb may occur during start-up and occasionally during steady-state power operation (e.g., due to ion exchanger resin intrusions or condenser leakages). The effect of sulphate and chloride, and in particular, of short-term chloride (5–50 ppb) and sulphate (50–370 ppb) transients (added as Na_2SO_4 or H_2SO_4 and NaCl or HCl, respectively) on the SCC crack growth behaviour was therefore mainly investigated with the high-sulphur RPV steels C and F in tests with periodical partial unloading (PPU) or constant static load in oxygenated high-temperature water (250–288 °C, 400 or 8000 ppb DO) [10,24,25].

Sulphate and sulphate transients: In oxygenated, high-temperature water (400 or 8000 ppb DO), the addition of up to 370 ppb of sulphate as Na_2SO_4 or H_2SO_4 (>'EPRI action level 3 limit') did not result in acceleration of crack growth under PPU and constant load in all materials. Under PPU conditions, the cracks were only growing during the rising load phase of the PPU cycles with only minor SCC crack growth during the subsequent constant load phases in both high-purity and sulphate containing water (Fig. 10(b)). Similarly, fast growing EAC cracks, triggered by cyclic or slow rising loading, arrested immediately after switching to constant load at stress intensity factors of up to 60 MPa $m^{1/2}$. The same crack growth behaviour as described above has also been observed by Materialprüfungsanstalt (MPA) Stuttgart in the framework of the CASTOC programme [18] at much higher sulphate contents of up to 1400 ppb (ca. 10 μS/cm). In all cases, the SCC CGRs under constant load during sulphate transients were conservatively covered by the 'BWRVIP-60 SCC disposition line 2' (Fig. 19).

In spite of the absence of any accelerating effect on SCC under highly oxidizing BWR conditions, sulphate still remains a harmful species for EAC in LAS, since it has been observed to affect EAC initiation from smooth surfaces in LCF and SSRT tests and to accelerate corrosion fatigue crack growth under reducing PWR conditions [10].

Chloride and chloride transients: In contrast to sulphate, our investigations clearly revealed that the addition of very small amounts of chloride as NaCl or HCl in the range of 5–15 ppb were already sufficient to induce fast SCC crack growth in RPV steels in oxygenated high-temperature water conditions (ECP $\geqslant 0$ mV_{SHE}) down to very low stress intensity factors of 20 MPa $m^{1/2}$ (Figs. 20 and 23).

In tests with periodical partial unloading (to 80% of maximum load every 12 h), acceleration of SCC crack growth was already observed a few hours after the addition of chloride in some cases. In pure constant load tests with a

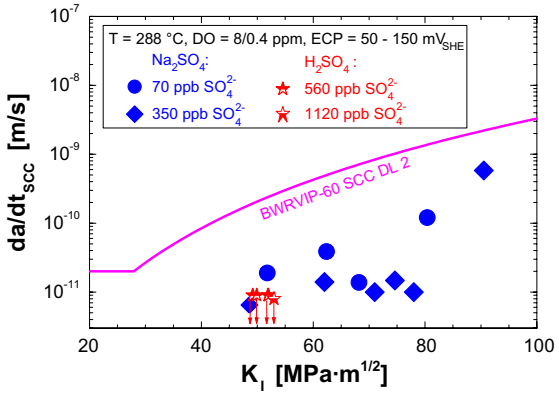

Fig. 19. Comparison of SCC CGRs during sulphate transients with the BWRVIP-60 SCC DL 2 for water chemistry transients.

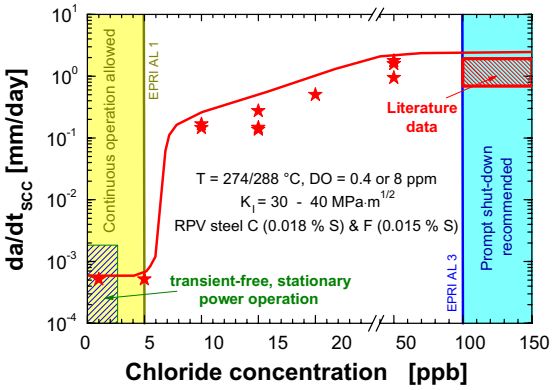

Fig. 20. Effect of chloride concentration on SCC crack growth rate in the high-sulphur reactor pressure vessel steel C under highly oxidizing BWR/NWC conditions (ECP = +50–150 mV_{SHE}) and comparison with action level 1 and 3 range of the EPRI water chemistry guidelines. These investigations indicate a critical chloride concentration in the range of 5–10 ppb slightly above the action level limit 1 for the investigated reactor pressure vessel steel in the stress intensity factor range of 30–40 MPa $m^{1/2}$.

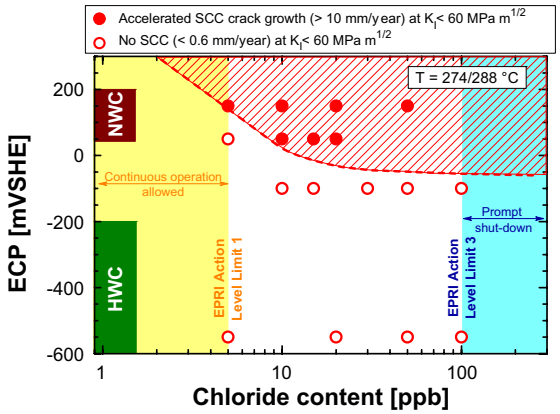

Fig. 21. Synergistic effect of corrosion potential ECP and chloride content on the onset of fast SCC crack growth in reactor pressure vessel steels under BWR conditions and comparison with the typical conditions during stationary power operation. Increasing chloride tolerance with decreasing ECP.

non-growing 'dormant' crack in high-purity water, a single partial un-/reloading cycle was necessary and sufficient for the onset of fast SCC crack growth during the chloride transient. The stationary SCC crack growth rates during the chloride transients reached up to 1.5 mm/day at high chloride levels of 50 ppb and significantly exceeded the 'BWRVIP-60 SCC disposition line 2' for water chemistry transients for chloride concentrations $\geqslant$5 ppb (Fig. 23, Section 5). A modification of the 'BWRVIP-60 SCC disposition line 2' should therefore be pursued for the case of chloride transients.

After returning to high-purity water, the cracks were still growing with the same high crack growth rates for some 10–50 h before a decay of the crack propagation rate was observed. In case of moderate chloride transients ($\leqslant$10 ppb), the SCC crack growth rates then dropped again to the same low values as in high-purity water (<0.6 mm/year) and below the 'BWRVIP-60 disposition line 1' for transient-free, stationary power operation within some few further hundreds of hours. After severe ($\geqslant$20 ppb) and prolonged (>100 h) chloride transients sustained, fast SCC crack growth was observed for at least 1000 h.

The critical chloride concentration for the onset of fast SCC significantly increased with decreasing ECP. This result thus indicates a significantly higher impurity tolerance at lower potentials (e.g., in the feedwater piping system) or under HWC conditions (Fig. 21).

Although the observations are only valid for long cracks, where enrichment of chloride in the crack-tip electrolyte by ion migration occurs [7,10] and may therefore not be directly transferred to defect-free component surfaces, they clearly show that much smaller chloride concentrations than believed so far can have a tremendous impact on SCC and that it is essential to maintain a low impurity level, in particular at high ECPs under NWC conditions. The possibly short incubation period for acceleration of SCC in combination with the very high SCC crack growth rates under static loading conditions of up to 1.5 mm/day and possible long-term effects, at least after severe ($\geqslant$20 ppb) and prolonged (>100 h) chloride transients, arise some concern for severe chloride transients under BWR/NWC conditions. The frequency and extent of chloride transients above the 'EPRI action level 1 limit' should therefore be reduced to the lowest possible level by adequate countermeasures and immediate actions.

5. Assessment of BWRVIP-60 SCC disposition lines

The conservative character of the 'BWRVIP-60 disposition line 1' for SCC crack growth in LAS has been confirmed by this and several other independent studies [10–15] for temperatures in the range of 274–288 °C and RPV base ($\leqslant$0.02 wt% S) and weld filler/heat-affected zone (HAZ) materials (Vickers hardness <350 HV5, $\leqslant$0.02 wt% S) if the water chemistry is maintained within current BWR/NWC operational practice (<'EPRI action level 1 limit') and the K_I value is below 60 MPa $m^{1/2}$. Even above 60 MPa $m^{1/2}$, most test results, in particular with low and medium sulphur RPV steels, were still below this curve as long as gross ligament yielding was avoided. The conservative nature of the approach was further confirmed by tests with periodical partial unloading (see Section 4.2.2) where cessation of SCC was observed for long hold times (>5–20 h) at constant load.

Several results indicated, however, that 'line 1' may be slightly exceeded at intermediate temperatures (180–270 °C) in RPV materials which show a distinct susceptibility to DSA (Fig. 22) [310, 15]. Furthermore, sustained SCC with CGRs significantly above 'line 1' was observed at 288 °C – not unexpectedly – when excessive hardness (>350 HV5) (e.g., in bad weld HAZs) was present in the steel [10,15], in particular in combination with a high steel sulphur content (Fig. 22).

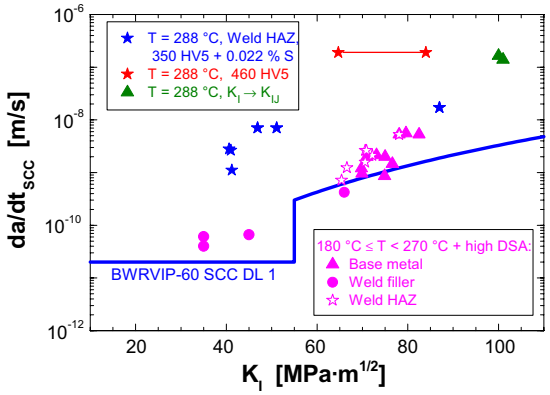

Fig. 22. Test results with SCC CGRs above the BWRVIP-60 SCC DL 1 [10,15].

Furthermore, the 'BWRVIP-60 SCC disposition line 2' may be significantly exceeded for the case of ripple loading ($R > 0.95$) [10,15] (Figs. 11 and 23) or with chloride transients ($\geqslant$'EPRI action level 1 limit') [10,24,25] (Figs. 20 and 23), even at fairly low stress intensity values around 20–30 MPa $m^{1/2}$. After severe ($\geqslant$20 ppb) and prolonged ($\geqslant$100 h) chloride transients, sustained SCC with CGRs above the 'line 2' was also observed in preliminary tests for a significantly longer time interval than the 100 h period specified in 'BWRVIP-60' [36, 67–69, 128] in case of highly oxidizing conditions (ECP $\geqslant$ 50 mV_{SHE}). On the other hand, 'line 2' seemed to conservatively cover even very severe sulphate transients relevantly above the 'EPRI action level 3 limit' values in both oxygenated and hydrogenated high-temperature water (Figs. 19 and Fig. 27) [10,24].

Laboratory experience has thus shown that fast SCC can only occur under some very specific conditions, which usually appear atypical for current BWR power operation practice or properly fabricated and heat-treated modern LAS components. Combinations of several of the following unfavourable factors can lead to sustained SCC with CGRs above the 'BWRVIP-60 SCC disposition lines' [10–15]:

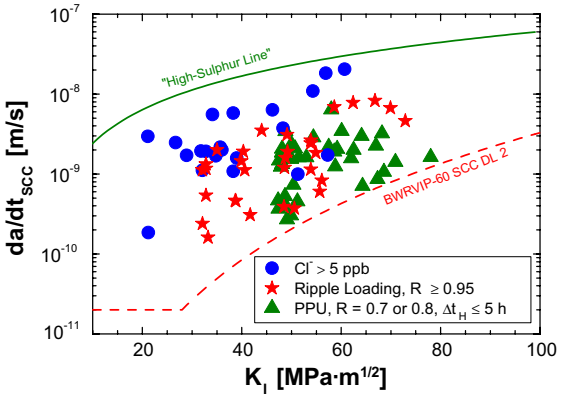

Fig. 23. Test results with SCC CGRs above the BWRVIP-60 SCC DL 2 [10,15].

- A high corrosion potential ECP > +100 mV_{SHE}/high DO content ($\gg$200 ppb) and quasi-stagnant flow conditions.
- Cl^- > 'EPRI action level 1 limit', $SO_4^{2-} \gg$ 'EPRI action level 3 limit'.
- A high steel sulphur content (>0.020 wt% S), in particular in combination with S-segregation zones.
- Intermediate temperatures (180–270 °C) in connection with distinct DSA susceptibility.
- A high hardness/YS level (>350 HV5, YS >800 MPa), e.g., in bad weld HAZs, in particular in conjunction with a high steel sulphur content.
- Loading close to K_{IJ} or severe violation of SSY conditions.
- Ripple loading or relatively frequent periodical partial unloading.

Under these unfavourable conditions, SCC CGRs can achieve rather high values, even up to a few m/year. The 'high-sulphur SCC line' of the General Electric model [7,14] gives a good estimate of the upper bound SCC CGR under such parameter combinations. Otherwise, the 'BWRVIP-60 SCC disposition line 1'' is conservative and adequate for the RPV during transient-free, steady-state BWR power operation at temperatures in the range from 270 to 290 °C. Some areas of potential concern remain to be evaluated, such as the RPV feedwater nozzle and feedwater piping systems with lower operating temperatures (200–270 °C) together with the possible occurrence of small load fluctuations (→ripple loading) and the case of chloride water chemistry transients.

6. Mitigation effect of hydrogen water chemistry

The mitigation effect of HWC was investigated under those critical parameter combinations, which generally revealed fast SCC with CGRs well above the 'BWRVIP-60 SCC disposition curves' under oxidizing NWC conditions. SCC tests with NWC (400 or 8000 ppb DO) → HWC (150 ppb DH) → NWC-transients always revealed a significant drop of the SCC CGR by a factor of at least 10 (up to 1000 under extreme situations) under static, ripple and periodical partial unloading conditions a few hours after adding hydrogen and changing to low potentials (<−200 mV_{SHE}). Therefore, a significant increase of safety margins is expected by the application of HWC with respect to NWC conditions. Under purely static loading and ripple loading conditions, the SCC CGRs remained on the very low HWC-level after returning to oxidizing NWC-conditions for the remaining test time of up to 1000 h. Under periodical partial unloading conditions, a few 10 h after returning to oxidizing NWC-conditions, the SCC CGR again reached the same high SCC CGR as before the HWC-transient [10,26].

As shown in Fig. 24, in the case of the susceptible weld HAZ material H, the application of HWC resulted in a significant reduction of the SCC CGRs under static load by

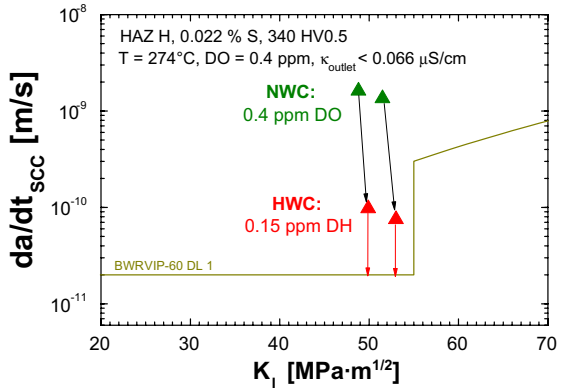

Fig. 24. Significant reduction of constant load SCC CGRs in the susceptible weld HAZ H by changing from oxidizing NWC (+60 mV_{SHE}) to reducing HWC (−580 mV_{SHE}) as indicated by the black arrows [26]. A few days after the transition to HWC conditions, the SCC CGRs of the initially stationary growing cracks started to continuously decrease as indicated by the red arrows.

more than a factor of 10 and a continuous decay of SCC CGRs at low potentials, thus also indicating cessation of crack growth on a long-term time scale.

Similarly, in the case of chloride transients in the concentration range of 5–50 ppb, the application of HWC also resulted in a significant drop of the SCC CGRs under static load a few hours after adding hydrogen and changing to low potentials (<−200 mV_{SHE}) and the CGRs dropped well below the 'BWRVIP-60 disposition line 2' for water chemistry transients. In Fig. 25, the SCC CGRs during chloride transients of 5 and 50 ppb in the RPV steels C and F under static loading conditions at a stress intensity factor of K_I of 58 MPa $m^{1/2}$ under NWC and HWC conditions are compared to the corresponding CGRs in high-purity water (<1 ppb Cl^-), which is characteristic for stationary power operation. These investigations clearly demonstrated a higher impurity tolerance under HWC conditions. The critical chloride concentration for the onset of accelerated SCC crack growth (>10 mm/year) at stress

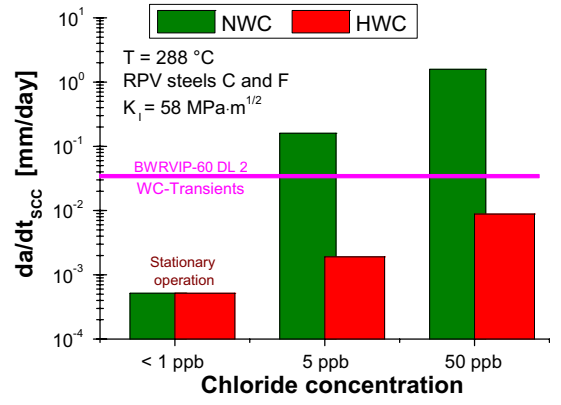

Fig. 25. SCC CGRs during chloride transients under NWC (ECP = +50 to +150 mV_{SHE}) and HWC (ECP = −620 mV_{SHE}) conditions and comparison to typical CGRs in high-purity water [26].

intensity factors K_I < 60 MPa $m^{1/2}$ under HWC conditions is expected to lie above 100 ppb and is therefore significantly higher than the relatively low values of 5 (+150 mV_{SHE}) to 10 ppb (+50 mV_{SHE}) at high potentials under NWC conditions (Fig. 26). This is due to the fact that no potential-gradient driven anion enrichment in the crack enclave is expected under HWC conditions [10].

Experiments with periodical partial unloading and ripple loading with the high sulphur RPV steel C and weld HAZ material H further confirmed the beneficial mitigation effect of HWC on SCC crack growth under critical system conditions (Fig. 26).

In high-purity, hydrogenated (150 ppb DH) high-temperature water (simulated BWR/HWC conditions) at 274 or 288 °C either no or very slow SCC crack growth well below the 'BWRVIP-60 disposition line 1' was observed under static load up to very high K_I values near to 100 MPa $m^{1/2}$ or to K_{IJ} (Fig. 27). After switching from cyclic to constant load, the SCC crack growth very quickly slowed down to CGRs of less than 0.6 mm/year within very few 10 h at K_I-values <60 MPa $m^{1/2}$. In contrast to oxygenated high-temperature water, where crack arrest was usually observed in this K_I-range, the DCPD measurement

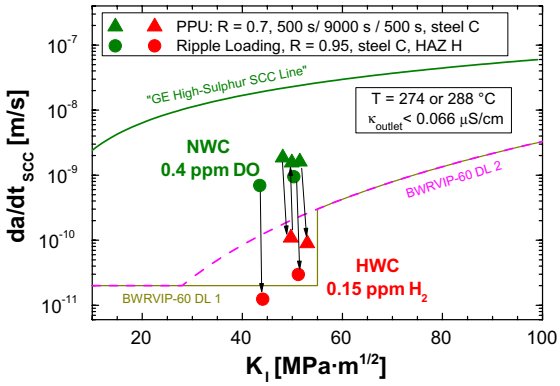

Fig. 26. Significant reduction of SCC CGRs under ripple and periodical partial unloading (PPU) conditions by changing from oxidizing NWC (ECP = +50–60 mV_{SHE}) to reducing HWC (ECP = −580 to −620 mV_{SHE}) as indicated by the arrows [26].

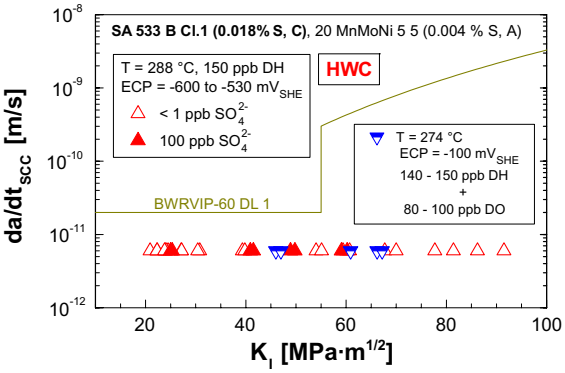

Fig. 27. Comparison of SCC CGRs under simulated BWR/HWC conditions with BWRVIP-60 SCC DL 1.

indicated that the cracks in hydrogenated water were often further growing after this transition phase with a very slow, but stationary rate in the range of 0.1–0.3 mm/year. This behaviour and the very conservative character of the 'BWRVIP-60 disposition line 1' for HWC conditions was further confirmed by tests with oxygen/hydrogen mixtures with a stoichiometric hydrogen excess at an increased ECP of $-100\,mV_{SHE}$ in high-purity or sulphate containing (100 ppb) high-temperature water (Fig. 27).

Based on these investigations, technically significant SCC crack growth during stationary BWR/HWC operation in low-alloy RPV and piping steels can be excluded in the ECP-range of -600 to $-200\,mV_{SHE}$ even in high-temperature water with a high sulphate or chloride content of 100 ppb (='EPRI action level 3 limit') up to high K_I-levels of at least 60 MPa $m^{1/2}$.

7. Summary and conclusions

The SCC crack growth behaviour of different RPV steels and weld filler/HAZ materials was characterized under simulated BWR/NWC and HWC conditions by periodical partial unloading, constant and ripple load tests with pre-cracked fracture mechanics specimens. The experiments were performed in oxygenated or hydrogenated high-purity or sulphate/chloride containing water at temperatures from 150 to 288 °C and revealed the following important results:

SCC crack growth behaviour: In excellent agreement with field experience, these investigations revealed a very low susceptibility to SCC crack growth and small crack growth rates (<0.6 mm/year) under most BWR/NWC and material conditions up to high stress intensity factors of 60 MPa $m^{1/2}$. Critical water chemistry (e.g., chloride content >5 ppb + high ECP > 0 mV_{SHE}), loading (e.g., ripple loading) and material (e.g., hardness >350 HV5, high DSA susceptibility + intermediate temperatures) conditions, which can result in sustained and fast (>10 mm/year for $K_I < 60$ MPa $m^{1/2}$) SCC under BWR/NWC conditions were identified, but many of them generally appeared atypical for current optimized BWR power operation practice or modern, properly fabricated RPVs. Application of HWC always resulted in a significant reduction of SCC crack growth rates by more than one order of magnitude under these critical system conditions and SCC CGRs dropped below the corresponding 'BWRVIP-60 disposition lines' some few hours after changing to HWC conditions.

BWRVIP-60 SCC disposition lines: The conservative character of the 'BWRVIP-60 disposition line 1' for SCC crack growth in LAS under NWC conditions has been confirmed for temperatures in the range of 274–288 °C and RPV base ($\leqslant$0.02 wt% S) and weld filler/HAZ materials (Vickers hardness <350 HV5, $\leqslant$0.02 wt% S) if the water chemistry is maintained within current BWR/NWC operational practice (<'EPRI action level 1 limit').

In case of NWC conditions, several results clearly indicated, however, that 'line 1' may be slightly exceeded at intermediate temperatures (180–270 °C) in RPV materials which show a distinct susceptibility to DSA. Furthermore, sustained SCC with CGRs significantly above 'line 1' was observed at 288 °C – not unexpectedly – when excessive hardness ($\geqslant$350 HV5) was present in the steel, e.g., in bad weld HAZ. Furthermore, the 'BWRVIP-60 disposition line 2' has been significantly exceeded for the case of ripple loading ($R > 0.95$) or during chloride transients ($\geqslant$'EPRI action level 1 limit'), even at fairly low stress intensity values around 30 MPa $m^{1/2}$. On the other hand, 'line 2' seemed to conservatively cover even very severe sulphate transients above the 'EPRI action level 3 limit'.

In case of HWC conditions, the 'BWRVIP disposition line 1' usually conservatively covers the SCC crack growth in LAS under the critical system conditions mentioned above.

Acknowledgements

The data of this paper have been generated within the SpRK, RIKORR and the CASTOC projects. The financial support for these projects by the Swiss Federal Nuclear Safety Inspectorate (HSK), the Swiss Federal Office of Energy (BFE), Swissnuclear and the Swiss Federal Office for Education and Science (BBW) is gratefully acknowledged. Thanks are also expressed to U. Ineichen, U. Tschanz, B. Gerodetti, and E. Groth (all PSI) for their experimental contribution to this work.

References

[1] B.M. Gordon, D.E. Delwiche, G.M. Gordon, ASM-PVP 119 (1987) 9.
[2] T. Matsunaga, K. Matsunaga, in: Proceedings of 11th International Conference on Nuclear Engineering, Shinjuku, Tokyo, Japan, April 20–23, 2003, CD-ROM, Paper ICONE11-36056.
[3] A. Yamashita et al., in: Proceedings of 9th International Conference on Nuclear Engineering, Nice, France, April 8–12, 2001, CD-ROM, Paper ICONE 9-66.
[4] R.M. Horn, P.L. Andresen, J. Hickling, in: 5th International Symposium on Contribution of Materials Investigation to the Resolution of Problems Encountered in Pressurized Water Reactors (Fontevraud 5), CD-ROM, Fontevraud, France, September 23–27, 2002, Paper No. 120.
[5] H.P. Seifert, S. Ritter, J. Hickling, Power Plant Chem. 6 (2) (2004) 111.
[6] Y.S. Garud et al., EPRI Report TR-106696, Electric Power Research Institute, Palo Alto, CA, USA, 1997.
[7] F.P. Ford, EPRI Report NP-7473-L, Electric Power Research Institute, Palo Alto, CA, USA, 1992.
[8] P. Scott, D. Tice, Nucl. Eng. Des. 119 (1990) 399.
[9] J. Hickling, D. Blind, Nucl. Eng. Des. 91 (1986) 305.
[10] H.P. Seifert, S. Ritter, SKI-Report 2005:60, ISSN 1104-1374, Swedish Nuclear Power Inspectorate, SKI, Stockholm, Sweden, 2005. (www.ski.se).
[11] J. Heldt, H.P. Seifert, Nucl. Eng. Des. 206 (2001) 57.
[12] K. Kussmaul, D. Blind, V. Läpple, Nucl. Eng. Des. 168 (1997) 53.
[13] F.P. Ford et al., in: Proceedings of 9th International Conference on Environmental Degradation of Materials in Nuclear Power Systems – Water Reactors, ANS/NACE/TMS, Newport Beach, CA, USA, August 1–5, 1999, p. 855.
[14] F.P. Ford, P.L. Andresen, NACE Corrosion 89, NACE, New Orleans, Houston, USA, Paper No. 498, p. 498-1.
[15] H.P. Seifert, S. Ritter, in: Proceedings of 11th International Conference on Environmental Degradation of Materials in Nuclear Power

Systems – Water Reactors, CD-ROM, NACE/TMS/ANS, Stevenson, WA, USA, August 10–14, 2003, p. 341.
[16] B. Cheng et al., EPRI TR-103515-R1, Electric Power Research Institute, Palo Alto, CA, USA, December 1996.
[17] M. Lasch, U. Staudt, VGB-Kraftwerkstechnik 75 (1995) 745.
[18] A. Roth et al., in: Proceedings of 12th International Conference on Environmental Degradation of Materials in Nuclear Power Systems – Water Reactors, CD-ROM, NACE/TMS/ANS, Snowbird, Utah, USA, August 14–18, 2005, p. 471.
[19] D. Blind et al., in: Proceedings of 9th International Conference on Environmental Degradation of Materials in Nuclear Power Systems – Water Reactors, ANS/NACE/TMS, Newport Beach, CA, USA, August 1-5, 1999, p. 911.
[20] U. Ehrnstén et al., in: Proceedings of 11th International Conference on Environmental Degradation of Materials in Nuclear Power Systems – Water Reactors, CD-ROM, NACE/TMS/ANS, Stevenson, WA, USA, August 10–14, 2003, p. 330.
[21] H.P. Seifert, S. Ritter, SKI Report 2005:60, ISSN 1104-1374, Swedish Nuclear Power Inspectorate, SKI, Stockholm, Sweden, 2005 (www.ski.se).
[22] H.M. Chung et al., NUREG/CR-4667, vol. 14, Argonne National Laboratory, August 1992.
[23] H. Hänninen, H.P. Seifert, Y. Yagodzinsky, U. Ehrnstén, O. Tarasenko, P. Aaltonen, in: Proceedings of 10th International Conference on Environmental Degradation of Materials in Nuclear Power Systems – Water Reactors, NACE/TMS/ANS, CD-ROM, Paper No. 47, Lake Tahoe, Nevada, USA, August 6–10, 2001, paper no. 0047.
[24] S. Ritter, H.P. Seifert, Power Plant Chem. 6 (12) (2004) 748.
[25] H.P. Seifert, S. Ritter, Chimia 59 (2005) 944.
[26] H.P. Seifert, S. Ritter, in: Proceedings of 12th International Conference on Environmental Degradation of Materials in Nuclear Power Systems – Water Reactors, CD-ROM, NACE/TMS/ANS, Snowbird, Utah, USA, August 14–18, 2005, p. 485.